Solar Energy Materials & Solar Cells 242 (2022) 111783

Contents lists available at ScienceDirect

Solar Energy Materials and Solar Cells

journal homepage: www.elsevier.com/locate/solmat

The impact of bead milling on the thermodynamics and kinetics of the structural phase transition of VO_2 particulate materials and their potential for use in thermochromic glazing

Lavinia Calvi [a,b], Romy van Geijn [c,d,e], Luc Leufkens [c,d], Roberto Habets [c,d], Kargal Laxminarayana Gurunatha [f], Kathleen Stout [e], Daniel Mann [c,d], Ioannis Papakonstantinou [f], Ivan P. Parkin [g], Ken Elen [a,b], An Hardy [a,b], Marlies K. van Bael [a,b], Pascal Buskens [a,c,d,*]

[a] Hasselt University, Institute for Materials Research (imo-imomec and Energyville), DESINe Group, Martelarenlaan 42, 3500, Hasselt, Belgium
[b] IMEC vzw, IMOMEC Associated Laboratory, Wetenschapspark 1, B-3590, Diepenbeek, Belgium
[c] The Netherlands Organisation for Applied Scientific Research (TNO), High Tech Campus 25, 5656AE, Eindhoven, the Netherlands
[d] Brightlands Materials Center, Urmonderbaan 22, 6167RD, Geleen, the Netherlands
[e] Zuyd University of Applied Sciences, Nieuw Eyckholt 300, 6400AN, Heerlen, the Netherlands
[f] Photonic Innovations Lab, Department of Electronic & Electrical Engineering, University College London, Torrington Place, WC1E 7JE, London, United Kingdom
[g] Department of Chemistry, University College London, 20 Gordon St, WC1H 0AJ, London, United Kingdom

ARTICLE INFO

Keywords:
Vanadium dioxide
Structural phase transition
Isoconversional kinetic analysis
Activation energy
Thermochromic
Coating
Bead milling

ABSTRACT

The thermodynamics and kinetics of the structural phase transition from monoclinic VO_2 (M) to rutile VO_2 (R) and *vice versa* were studied for particulate materials obtained by bead milling of VO_2 (M) powder. Using wet bead milling, we decreased the particle size of VO_2 (M) powder from ~1 μm to 129 nm. With progressive milling, the switching enthalpy decreased from 47 J g^{-1} to 29 J g^{-1} due to a loss of crystallinity. The switching kinetics were studied using Friedman's differential isoconversional method. The activation energy $|E_\alpha|$ decreases with increasing difference between the actual temperature of the material and its switching temperature (T_0). Furthermore, $|E_\alpha|$ decreases with progressive milling, and kinetic asymmetry is induced. For milled particulate materials, $|E_\alpha|$ is lower for the switch from VO_2 (R) to VO_2 (M) than for the opposite switch. For hydrothermally synthesized nanoparticles, $|E_\alpha|$ is in the same order of magnitude, albeit with inverse switching asymmetry. Latter may result from different defects that are introduced during both preparation techniques. Applying layers of milled particulate material to glass sheets yielded thermochromic coatings with luminous transmission of 40.7% and solar modulation of 8.3%. This demonstrates that milled VO_2 particles have potential for use in energy efficient thermochromic windows.

1. Introduction

The interest in monoclinic vanadium dioxide – VO_2 (M) – is high because of its thermochromic properties, which can be tailored for a range of applications [1–5]. VO_2 (M) undergoes a structural phase transition (SPT) to rutile VO_2 (R) with a tetragonal unit cell at approximately 68 °C [6]. A first order metal-insulator transition (MIT) accompanies this SPT as VO_2 (M) is a semiconductor with high transmission for solar infrared (IR) light, whilst VO_2 (R) is an electrical conductor that absorbs and reflects IR radiation. Integration of VO_2 (M) into a film or coating for application in smart thermochromic windows can lead to a significant reduction in energy consumption for heating and cooling of buildings in intermediate climates [7,8].

A key challenge for successful implementation of VO_2 (M) in coatings and polymer films for smart windows is achieving both a high luminous transmittance (T_{lum}) and a high modulation of solar energy (ΔT_{sol}) [9,10]. T_{lum} is low (~40%) for both VO_2 (M) and VO_2 (R) [2,11], as a large portion of the visible light is either absorbed or reflected [12,13], and ΔT_{sol} is also low (~10%) [2,14]. Increasing ΔT_{sol} generally leads to a decrease in T_{lum} and *vice versa* [15–17]. To increase both T_{lum} and ΔT_{sol}, the concept of nanothermochromic films was proposed by Granqvist and coworkers [15,18–22]. Their optical simulations show that higher T_{lum}

* Corresponding author. The Netherlands Organisation for Applied Scientific Research (TNO), High Tech Campus 25, 5656AE, Eindhoven, the Netherlands.
E-mail address: pascal.buskens@tno.nl (P. Buskens).

https://doi.org/10.1016/j.solmat.2022.111783
Received 4 March 2022; Received in revised form 26 April 2022; Accepted 29 April 2022
Available online 11 May 2022

and ΔT_{sol} can be achieved when using thermochromic nanoparticles [18]. In order for the nanoparticles to achieve the increase in both parameters the following key requirements need to be met: particle sizes far below visible light wavelength (≤100 nm) to avoid scattering of visible light, particles randomly dispersed in the film or coating, and high purity and crystallinity of particles to ensure good switching performance [20,23]. Therefore, high quality thermochromic nanoparticles with a switching temperature suited for application in smart windows (15–25 °C [7,24]) are of great interest. The suitable temperature can be achieved through oxygen vacancies (point defects), doping with different elements and strain in the crystal lattice [25,26].

Bead milling of VO_2 (M) powders is a top-down approach which holds the potential to yield large quantities of such material. Multiple groups have prepared undoped and doped VO_2 nanoparticles using bead milling, and applied them to produce thermochromic coatings and films [25,27–29]. In previous research Liu et al. [30] carried out wet bead milling of VO_2 powder in dipropylene glycol methyl ether with the addition of Disperbyk 180 as dispersing agent for 4 h using zirconia beads at 4200 rpm. They obtained particles of a size below the wavelength of visible light, and measured particle sizes of about 300 nm in dispersion using dynamic light scattering (DLS), and 20–50 nm in dry state using transmission electron microscopy (TEM). They dispersed the obtained nanoparticles in a silica-alumina gel and subsequently casted that on a float glass substrate. The best balance of properties was achieved with a gel layer thickness of 3.0 μm, yielding T_{lum} of 59% and ΔT_{sol} of 12%. Based on peak broadening in the X-ray diffractograms (XRD) of VO_2 nanoparticles, Liu et al. proposed that bead milling reduced the crystal size of VO_2 without distorting the crystal structure leading to retention of the thermochromic properties. Kim et al. [31] carried out the synthesis of VO_2 nanoparticles by wet bead milling of V_2O_5 powder in ethanol using polyvinylpyrrolidone (PVP) as dispersant and 0.2 mm zirconia beads for 18 h at 3000 rpm. After milling, the amorphous V_2O_5 nanoparticles were thermally treated at 500 °C in a nitrogen atmosphere. They claim that these conditions are suited to convert the nanoparticles to VO_2 (M), resulting in almost spherical nanoparticles in the size range of 30–60 nm, with a switching enthalpy of approximately 24 J g^{-1} and peak temperatures of 87 °C and 58 °C for the switch from VO_2 (M) to VO_2 (R) and *vice versa*, respectively. Note: The peak temperature is defined as the temperature at the maximum of the differential scanning calorimetry (DSC) peak. Critical switching temperature (T_0) is the lowest temperature at which VO_2 (M) switches to VO_2 (R). At this temperature the switch is infinitely slow. $T_{\alpha = 0.02}$ is the temperature at 2% conversion of the VO_2 crystals, and is representative for T_0. $T_{\alpha = 0.50}$ is the temperature at a conversion of 50%, which is used for establishing the Friedman plot (*vide infra*) and typically does not coincide with the peak temperature. Kim et al. [31] attributed this increased switching temperature for VO_2 (M) to VO_2 (R) to the decrease in potential defects, therefore leading to an increase in the energy barrier for nucleation. The coatings comprising VO_2 (M) nanoparticles were prepared by tape-casting and the thick coating resulted in a T_{lum} of 43% and ΔT_{sol} of 7%. Wang et al. [20] bead milled hydrothermally synthesized VO_2 (B) nanobelts with three different zirconia bead sizes (10, 8 and 5 mm) to form VO_2 (M). After dry milling for 5 h at 1425 rpm, they obtained a particle size of 38 nm. The obtained nanoparticles were dispersed in a mixture of ethanol and polyvinyl butyral (PVB) to cast a film using a roller bar. The differential scanning calorimetry (DSC) peaks were broad and displayed an average switching enthalpy of 20 J g^{-1}. Both peak temperatures increased by 5–10 °C, and it was suggested that intermediate phases being present produce lattice stress and lower the phase transition temperature. The 2.5 μm thick film resulted in a thermochromic performance of T_{lum} of 67% and ΔT_{sol} of 8%. Wang et al. [32] hydrothermally synthesized branched VO_2, dispersed it in ethanol (94 wt%) and PVP (3 wt%) and bead milled the dispersion for 12h at 500 rpm, then performed spin coating with the milled dispersion. The thinnest coating exhibited a T_{lum} of 64% and ΔT_{sol} of 1% while the thickest coating yielded 20% and 4%, respectively. Chen et al. [33] hydrothermally synthesized W-doped VO_2 (M) nanoparticles (25–75 nm) and used bead milling to disperse the particles efficiently in a hydrophobic silicone resin in presence of butanol and a dispersant. Subsequently, the dispersion was roll coated on clear glass and dried, the optical properties of the coating are the following: T_{lum} of 53%, ΔT_{sol} of 16.6% and peak temperatures of 43 °C and 17 °C.

In spite of multiple studies on the preparation of (doped) VO_2 (M) nanoparticles produced by bead milling of powers and their application in coatings and films, a systematic study on the impact of bead milling on the thermodynamics (T_0 and enthalpy (ΔH)) and kinetics (activation energy (E_a)) of the SPT of micron and nanosized VO_2 particles has not yet been reported. Previously, we have studied the kinetics of VO_2 powders using isoconversional kinetic analysis, and demonstrated that the activation barrier was symmetric for the SPT from VO_2 (M) to VO_2 (R) and *vice versa*, and decreased with increasing difference between the material's temperature and T_0. [24] In the current manuscript, we systematically study the impact of bead milling on the thermodynamics (T_0 and ΔH) and kinetics (E_a) of undoped micron- and nanosized VO_2 particles. Furthermore, we compare the properties of the smallest milled nanoparticles to properties obtained with hydrothermally synthesized VO_2 nanoparticles of the same order of magnitude, and report the optical properties (T_{lum} and ΔT_{sol}) of layers of milled particles deposited on float glass using dip coating to demonstrate their application potential in thermochromic windows.

2. Experimental section

2.1. Preparation of VO_2 slurry

Vanadium(IV) oxide (VO_2, 80.0 g, 99% metal basis, Alfa Aesar, 100 mesh powder, contains V_6O_{13} as impurity) was dispersed in isopropanol (IPA, 270 g, VWR chemicals, technical) and sonicated in an ultrasonic bath for 15 min to yield a VO_2 slurry suited for bead milling.

2.2. Bead milling procedure

The VO_2 slurry was added to the Bühler PML 2 fitted with a MicroMedia™ L milling chamber, having an internal volume of 70 mL (Fig. S1). The milling camber was pre-filled with zirconium oxide beads (56 mL, 208 g, 80% of chamber volume, yttrium stabilized, 0.2 mm, Bühler, Draison®YUP) and IPA (138 g). After addition of the slurry and IPA (300 g) the total VO_2 content was 10 wt%. The rotations per minute and pump power were initially set to 1500 rpm and 80%, respectively, and then increased to 3000 rpm and 100% (Table S1 for flow rate). During milling the dispersion is kept at an operating temperature below 35 °C using water cooling. When the mill speed is increased to 3000 rpm the system modulates the speed when the temperature exceeds 35 °C to prevent it from overheating (Fig. S1). The system was continuously flushed with nitrogen to prevent oxidation of VO_2 during milling. Samples were taken every 3000 kWh·t^{-1}, diluted for DLS analysis (1 drop in 10 mL and ultrasonicated for 2 min in an ultrasonic bath) and dried in a vacuum oven at 40 °C for DSC, X-ray diffraction (XRD), TEM and scanning electron microscopy (SEM) analyses.

2.3. Procedure and data collection for the kinetics study

Differential Scanning Calorimetry (DSC) was carried out on a Discovery DSC (TA Instruments) using Tzero aluminium pans containing 20 mg of dried sample. All the samples were subjected to the following six heating and cooling rates: 1.5, 5, 7.5, 10, 15 and 20 °C·min^{-1}. Before data collection all DSC pans where subjected to 4 cycles of heating and cooling at 20 °C·min^{-1} from 0 to 120 °C to ensure that the samples where completely dry. After this procedure, the sample mass was determined again. For analysis a DSC was used from TA instruments fitted with TRIOS software v5.1, the data collected were analysed and processed in accordance with the isoconversional method, which is

discussed in section 3.1.

2.4. Fabrication of thermochromic coating

The dispersion consisting of VO_2 nanoparticles was placed in a small dip tank (~2.53 wt% VO_2 in IPA). Then, a clean glass plate (4 mm thick) was clamped and the glass was immersed in the dispersion at a rate of 10 mm s^{-1} and retracted at a speed of 8 mm s^{-1} using a dip coater custom built by KOM Engineering and Assembling B.V. (Fig. S2). After drying at ambient conditions, the optical properties of the thermochromic coating were determined using UV–vis–NIR spectrophotometry (*vide infra*).

2.5. Hydrothermal synthesis of VO_2 nanoparticles

Hydrazine hydrate ($N_2H_4{\cdot}H_2O$) is an effective reagent to hydrothermally synthesize VO_2 nanoparticles by reduction of V_2O_5 [34,35]. V_2O_5 (182.0 mg, 1.00 mmol, 99.99%, Sigma Aldrich) was added to a solution of H_2O_2 (7.00 mL, 20.6 mmol, 30 wt%, Fischer Scientific) preheated at 60 °C with stirring. After vigorous bubble formation, a dark brown vanadium(V) peroxo complex was formed and the reaction was continued for 1 h followed by the addition of DI water (12.0 mL). This solution was then treated with $N_2H_4{\cdot}H_2O$ (36.0 μL, 0.74 mmol), and the resulting mixture was immediately sealed in a 45 mL Teflon-lined autoclave (Parr 45 mL Autoclave, model 4744). The hydrothermal reaction was performed at 220 °C for 72 h by placing the autoclave in an oven. After cooling, the solid product was collected, washed with copious amounts of DI water and ethanol, and isolated by centrifugation (10k rpm). Ultimately, the product was dried in a vacuum oven at 50 °C for 12 h. Caution: The reaction of V_2O_5 with H_2O_2 is highly exothermic! Therefore, precaution must be taken while carrying out the reaction, and during the hydrothermal reaction the total volume of the reactants must never exceed 45% of the capacity of the Teflon autoclave.

2.6. Characterization techniques

X-ray diffraction (XRD) measurements to determine the composition of the vanadium oxide particulate materials were carried out on a Bruker D8 Advance. Scanning transmission electron microscopy – energy dispersive X-ray (STEM-EDX) analyses were performed using a probe-corrected JEOL ARM 200F operated at 200 kV, equipped with a 100 mm^2 SDD EDS detector. The method used was High Angle Annular Dark Field (HAADF) STEM, and EDX, spot 3 C. The TENEO Scanning Electron Microscope (SEM) was used for obtaining images of the milled VO_2 particulate materials. The measurements of the thermochromic coatings were carried out using a PerkinElmer Lambda 750 UV–vis–NIR spectrometer equipped with a temperature-controlled module manufactured by OMT Solutions B.V. for measuring transmission at temperatures between 0 °C and 120 °C (Fig. S3). A Bruker NPFlex white light interferometer in vertical scan (VSI) mode with a 50x objective was used to measure the coating thickness.

3. Results and discussion

3.1. Characterization of VO_2 particulate materials obtained by bead milling

To obtain sub-micron sized VO_2 particulate materials, we prepared a slurry of commercially available VO_2 powder in isopropanol (IPA). This slurry was then subjected to bead milling using yttrium-stabilized zirconia beads with a size of 0.2 mm. During milling, the system was cooled with water to ensure a maximum operating temperature of 35 °C. Furthermore, milling was performed in a nitrogen atmosphere to avoid oxidative degradation of VO_2 during the process. Every 3000 kWh milling energy per ton (kWh·t^{-1}) of VO_2 (M), product samples were taken for characterization. SEM analyses of these samples were performed to determine the evolution of size and shape of the particles during milling (Fig. 1a–d, Fig. S4). The size was determined using Martin's diameter method by measuring the length and width of each particle [36]. On average 125 particles were measured for each sample. The unmilled powder consists of large polydisperse flakes with a particle size of 0.96 ± 0.20 μm (Fig. 1a, Fig. S5). After 3000 kWh·t^{-1} milling energy, the flake-like particles were reduced in size to 242 ± 59 nm (Fig. 1b). After 9000 kWh·t^{-1} and 13000 kWh·t^{-1} the particle size was reduced to 159 ± 34 (Figs. 1c) and 129 ± 27 nm (Fig. 1d), respectively. In addition to SEM, we also performed DLS analyses to determine the particle size in dispersion (Fig. S6). For the unmilled particles, the average size obtained by DLS (436 nm, Fig. S6) was roughly 15 times smaller than the particle size obtained by SEM (6.35 μm). This discrepancy is caused by sedimentation of larger particles during the DLS analysis. For the milled samples, the average particle size obtained by DLS is in good agreement with the particle size obtained by SEM (Fig. S6).

As means to assess the purity of the unmilled VO_2 (M) powder and the milled particulate materials, the switching enthalpy ΔH was determined by DSC analyses (Fig. 1e). ΔH of the unmilled VO_2 (M) powder was 46.8 J g^{-1} (Fig. 1f, Table 1), which is slightly lower than expected for a pure VO_2 (M) powder [6,37–39]. XRD analysis revealed that this was caused by the presence of V_6O_{13} as an impurity (Fig. S7). Upon milling, the maximum of the DSC peaks decreased and the peaks also broadened. With progressive milling, ΔH decreased to 43.3 J g^{-1} (3000 kWh·t^{-1}), 31.9 J g^{-1} (9000 kWh·t^{-1}) and 29.1 J g^{-1} (13000 kWh·t^{-1}, Table 1). Furthermore, we observed a decrease in T_0 for the switch from VO_2 (M) to VO_2 (R) from 65.03 °C (unmilled) to 64.45 °C (3000 kWh·t^{-1}), 59.17 °C (9000 kWh·t^{-1}) and 55.93 °C (13000 kWh·t^{-1}). For the switch from VO_2 (R) to VO_2 (M), we observed an increase from 71.03 °C (unmilled) to 74.81 °C (3000 kWh·t^{-1}), 84.86 °C (9000 kWh·t^{-1}) and 88.51 °C (13000 kWh·t^{-1}). This results in an increase in width of the switching hysteresis from 6.00 °C (unmilled) to 10.36 °C (3000 kWh·t^{-1}), 22.84 °C (9000 kWh·t^{-1}) and 32.58 °C (13000 kWh·t^{-1}). Note: the hysteresis is defined as the difference between the T_0 values of both switches [24].

To investigate the reduction in ΔH upon milling, we performed XRD analyses to determine the crystalline components in the bead milled samples (Fig. S7). All milled and unmilled particulate samples consisted of VO_2 (M) with an impurity of V_6O_{13}. No oxidized materials were detected within the detection limit of the equipment, which confirms that bead milling under nitrogen atmosphere effectively prevents oxidative degradation. To determine the degree of crystallinity of the bead milled particulate materials, we performed Global Rietveld refinement analysis of the XRD patterns using DIFFRAC.TOPAS (Bruker) for profile fitting (SI7) [40]. These clearly show an increase in amorphous fraction from 0 to 10% for the unmilled material to 20–40% for milled particulate materials (Table S7), which explains the 33% decrease in ΔH when comparing the unmilled powder to the material obtained after milling (13000 kWh·t^{-1}). To independently validate the presence of amorphous material in the milled samples, we performed brightfield (BF) and high resolution (HR) TEM analyses (Fig. 2). For that purpose, we separated large and small particles present in dispersion after milling (13000 kWh·t^{-1}) using centrifugation. The larger particles, which formed the pellet sediment during centrifugation, were largely crystalline (Fig. 2b, e). The particles' crystallite orientations were not all aligned, many small grains were present. Furthermore, the crystallinity seemed to extend to the surface of the grain and amorphous regions could not be detected. The material present in the supernatant after centrifugation appeared porous and fibrous in nature, and no crystalline regions could be detected (Fig. 2c, f, Fig. S8). These observations were confirmed by DSC analyses of the dried pellet and supernatant, resulting in good switching performance of the material in the pellet ($\Delta H = 30.9$ J g^{-1}, Fig. S9) and poor switching performance of the material in the supernatant ($\Delta H = 2.1$ J g^{-1}, Fig. S9). *Ergo*, we have unambiguously demonstrated a loss of crystallinity upon progressive milling by XRD and Rietveld analyses, TEM analysis (incl. elected area electron diffraction,

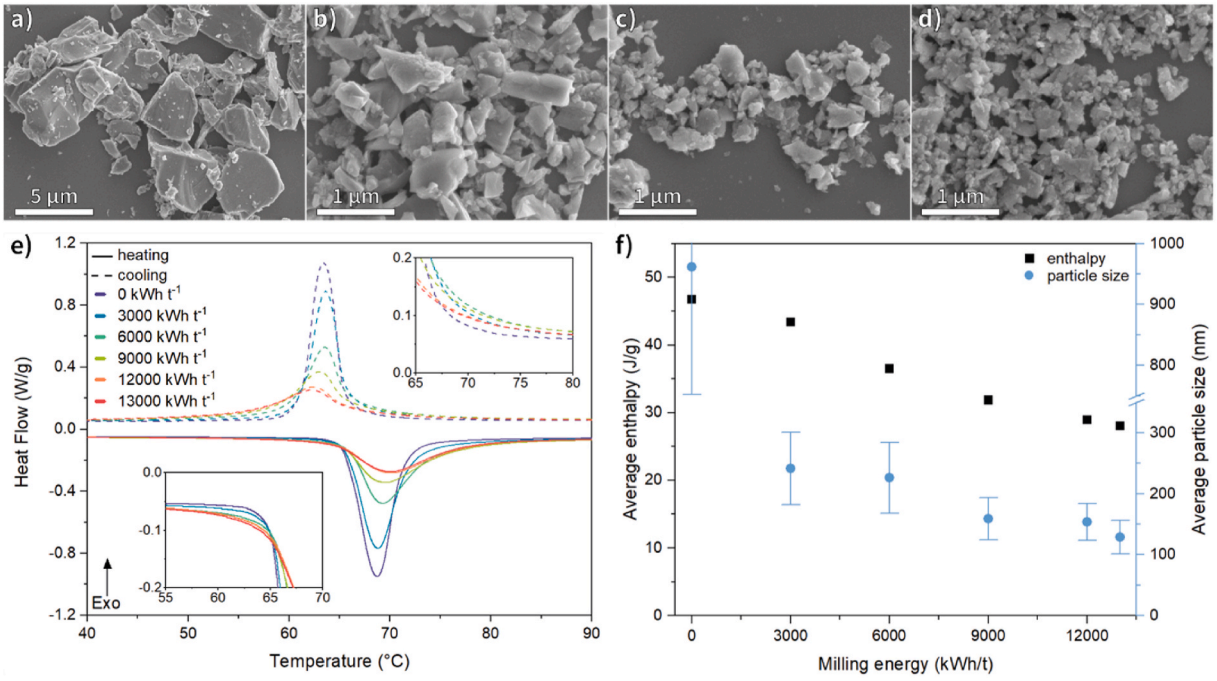

Fig. 1. a) SEM image of unmilled VO_2 (M) powder, b) SEM image of milled VO_2 (M) particulate material at 3000 kWh·t^{-1} energy input, c) SEM image of milled VO_2 (M) particulate material at 9000 kWh·t^{-1} energy input, d) SEM image of milled VO_2 particulate material at 13000 kWh·t^{-1} energy input, e) DSC of unmilled powder and milled VO_2 particulate materials at energy inputs ranging from 3000 to 13000 kWh·t^{-1} obtained at a heating rate of 5 °C·min^{-1} (with magnified inserts showing in detail the start of each switch), and f) average enthalpy of SPT and average particle size obtained by DSC and SEM analyses, respectively, as function of the milling energy.

Table 1
Temperature at 2% and 50% conversion of the unmilled VO_2 powder sample and milled VO_2 particulate samples obtained from DSC analysis at heating/cooling rate of 5 °C·min^{-1} and average switching enthalpy $<\Delta H>$ for all heating rates (1.5, 5, 7.5, 10, 15 and 20 °C·min^{-1}).

Milling energy [kWh·t^{-1}]	$T_{\alpha=0.02}$ [°C]		$T_{\alpha=0.50}$ [°C]		$<\Delta H>$ [J·g^{-1}]	
	VO_2 (M) to VO_2 (R)	VO_2 (R) to VO_2 (M)	VO_2 (M) to VO_2 (R)	VO_2 (R) to VO_2 (M)	VO_2 (M) to VO_2 (R)	VO_2 (R) to VO_2 (M)
0	65.03	71.03	68.37	63.89	46.8 ± 0.5	46.7 ± 0.3
3000	64.45	74.81	68.77	64.06	43.4 ± 0.4	43.2 ± 0.5
6000	59.55	82.39	69.93	63.83	36.5 ± 0.5	37.5 ± 0.9
9000	59.17	84.86	70.56	62.70	31.9 ± 0.6	33.3 ± 0.8
12000	56.13	86.45	70.84	62.19	28.9 ± 0.3	30.8 ± 0.6
13000	55.93	88.51	70.59	61.85	28.1 ± 0.2	31.0 ± 0.8

Fig. S8.1) and DSC analysis of the particulate mixture and separated fractions of large and small particles.

3.2. Thermokinetic analysis of milled VO_2 particulate materials

Very recently, we applied Friedman's differential isoconversional method [41,42] to study the kinetics of the SPT of undoped and W-doped VO_2 powders [24]. The principles of this study will be outlined below. During the VO_2 (M) to VO_2 (R) phase transition, and above T_0, nucleation occurs which is formation of small nuclei of the second phase within the initial phase. Growth and aggregation of the nuclei continues until homogeneity is reached [43,44]. Impurities and defects can facilitate the nucleation in solids as diffusion and aggregation within the lattice is facilitated [45]. The kinetics of the SPT can be represented by a single-step kinetic equation based on Arrhenius Law [41]:

$$\frac{d\alpha}{dt} = \mathrm{A}\ \ exp\left(\frac{-E}{RT}\right) f(\alpha) \tag{1}$$

Here A is a pre-exponential factor (temperature independent), E is the activation energy for the transition, R is the gas constant, T is temperature, $f(\alpha)$ is the reaction model and α is the degree of conversion ($0 \leq \alpha \leq 1$). Taking the reaction rate as the only temperature dependent parameter (isoconversional principle) leads to following relationship for the activation energy E_α [41]:

$$E_\alpha = -R\left(\frac{d\ln(d\alpha/dt)}{dT^{-1}}\right)_\alpha \tag{2}$$

Rearranging equation (1) leads to the foundation of the Friedman differential isoconversional method [41,42]:

$$-R\ln\left(\frac{d\alpha}{dt}\right)_{\alpha,i} = -R\ln(A_\alpha f(\alpha)) + \frac{E_\alpha}{T_{\alpha,i}} \tag{3}$$

where i indicates the different heating rates. Plotting $-Rln(d\alpha/dt)$ versus T^{-1} leads to the Friedman plot, where the gradient is the activation energy barrier for nucleation. The free energy barrier for the formation of a new nucleus (ΔG^*) corresponds to the activation barrier. Above the critical radius the nucleus grows spontaneously. Assuming it is spherical for homogeneous nucleation, then ΔG^* can be defined in the following manner [43]:

$$\Delta G^* = \frac{16\pi\sigma^3 T_0^2}{3(\Delta H)^2(\Delta T)^2} = \frac{A}{(\Delta T)^2} \tag{4}$$

where, T_0 is the critical temperature (where the switch is infinitely slow), ΔH is the phase transition enthalpy and σ is the surface energy of the nucleus. Since all these parameters are material constants, they can be combined into one integrated constant A. $\Delta T = T - T_0$ for heating and

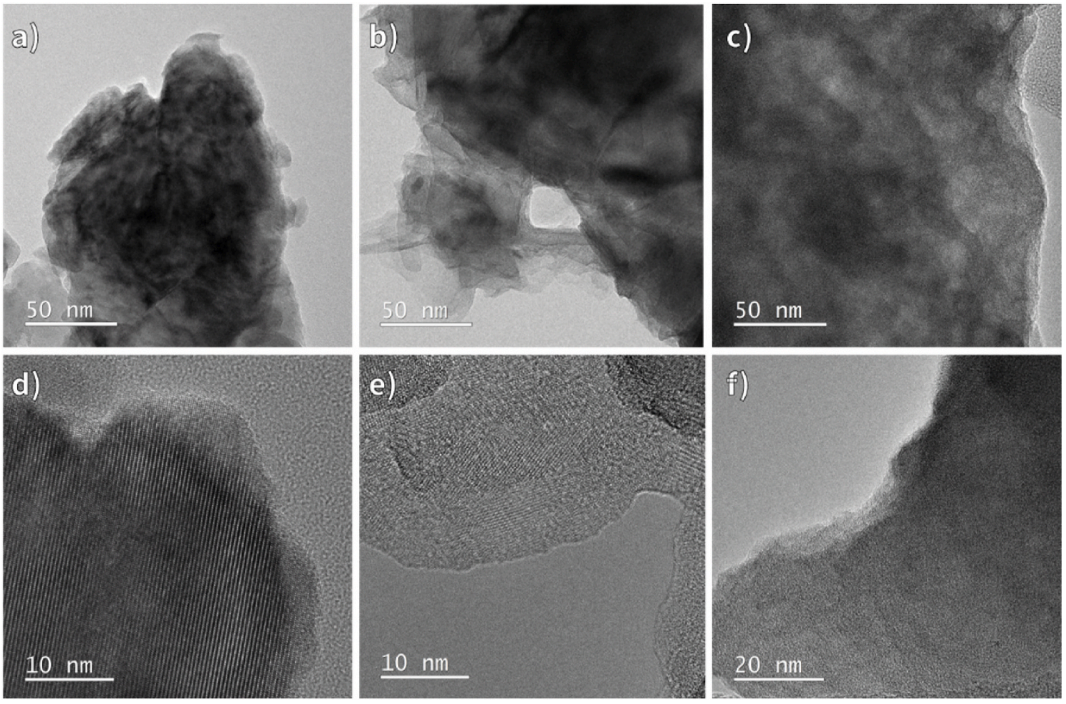

Fig. 2. a) BFTEM image of milled VO_2 particulate material, b) BFTEM of pellet after centrifugation, c) BFTEM of supernatant after centrifugation, d) HRTEM of milled VO_2 particulate material, e) HRTEM of pellet after centrifugation, f) HRTEM of supernatant after centrifugation. The milling energy input of the analysed materials was 13000 kWh·t^{-1}.

$\Delta T = T_0$ - T for cooling, where T is the material temperature. The value of T_0 is taken at a conversion of 2% and referred to as $T_{\alpha\ =\ 0.02}$. The Friedman plot results in a non-linear relationship, since ΔG^* depends on ΔT [43]. E_α depends on conversion as the single-step equation is only applicable to a specific α in the ΔT range [41]. Therefore the constant value of $\alpha = 0.50$ is used in our study.

Derivation of equation (3) and then substituting this into equation (2) gives the following two equations, E_h for heating and E_c for cooling:

$$E_h = A\left(\frac{1}{(\Delta T)^2} + \frac{2T}{(\Delta T)^3}\right) or\ E_c = A\left(\frac{1}{(\Delta T)^2} - \frac{2T}{(\Delta T)^3}\right) \quad (5)$$

In the following study, the extent of conversion equals the fractional enthalpy of the DSC peak, defining the nucleation rate [42].

$$\frac{d\alpha}{dt} = \frac{dH}{A_T dt} \quad (6)$$

where H is the enthalpy of the phase transition, A_T is the area under the entire thermogram, which is the enthalpy of the entire phase transition.

To study the kinetics of the SPT of unmilled powder, we performed DSC analyses using 6 different heating and cooling rates ranging from 1.5 °C·min^{-1} to 20 °C·min^{-1}. We converted the 6 DSC plots (Fig. 3a, only the SPT from VO_2 (M) to VO_2 (R) is plotted) into conversion-time profiles (Fig. 3b) and determined the temperature and reaction rate at 50% conversion for each heating and cooling rate. These were subsequently used to establish the Friedman plot (Fig. 3c). The same study was performed for the milled particulate materials (Fig. 4a).

By combining equation (4) and equation (3) the following relationship is derived:

$$-R\ln\left(\frac{d\alpha}{dt}\right) = -R\ln(\omega_0) + \frac{16\pi\sigma^2}{3(\Delta H)^2}\cdot\frac{T_0^2}{(\Delta T)^2 T} \quad (7)$$

Using equation (7) and the excel built-in solver the dataset was used to fit curves, the parameters for equation (7) are provided in Table S10. Using the values in equation (7), the gradient between two consecutive

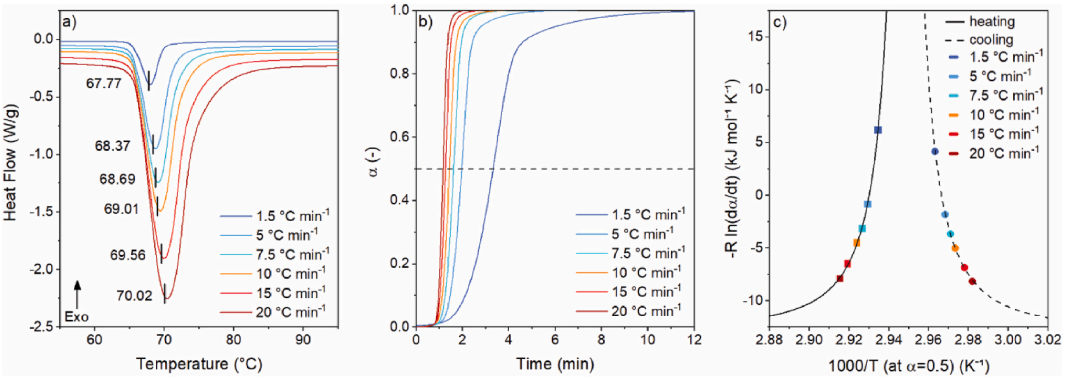

Fig. 3. a) DSC heating curves for unmilled VO_2 powder at different heating rates, the indicated values correspond to the temperature at $\alpha = 0.50$, b) Conversion-time profile of unmilled VO_2 (M) to VO_2 (R) at different heating rates (running integral of DSC curve with respect to time), and c) Friedman plot at $\alpha = 0.50$ for the unmilled VO_2 (M) to VO_2 (R) SPT and *vice versa*.

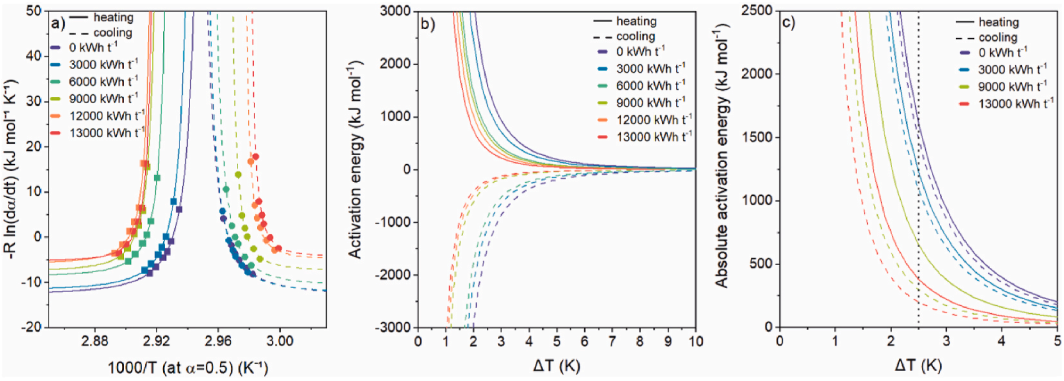

Fig. 4. a) Friedman plot for the unmilled VO_2 powder sample and milled VO_2 particulate materials at $\alpha = 0.50$ for the VO_2 (M) to VO_2 (R) SPT and *vice versa*, b) activation energy of the unmilled VO_2 powder sample and milled VO_2 particulate materials as function of ΔT, and c) absolute activation energy as function of ΔT.

points was used to derive the activation energy, and consecutively plot the activation energy as function of ΔT for the unmilled powder and milled particulate materials (Fig. 4b, Table 2). $|E_\alpha|$ depends on the temperature of the material and decreases rapidly with increasing ΔT (Fig. 4b) The switching kinetics of the unmilled powder are reasonably symmetric, with $|E_\alpha| = 1610$ kJ mol^{-1} for the SPT from VO_2 (M) to VO_2 (R) and $|E_\alpha| = 1491$ kJ mol^{-1} for the SPT from VO_2 (R) to VO_2 (M) at $\Delta T = 2.5$ °C. The Friedman plots for the unmilled and all milled samples clearly show that the switching temperatures change upon milling, and that the hysteresis width increases (as reported earlier in the manuscript). Furthermore, $|E_\alpha|$ decreases upon progressive milling, and the switching kinetics become increasingly asymmetric. The switching kinetics of the milled sample with 13000 kWh·t^{-1} milling energy displays the lowest $|E_\alpha|$ for the SPT from VO_2 (M) to VO_2 (R) and *vice versa*, viz. 381 and 202 kJ mol^{-1}, respectively, at $\Delta T = 2.5$ °C. The lowering of $|E_\alpha|$ is likely to be caused by surface defects introduced in the crystal during milling [46]. Apparently, the impact of these defects on the switch from VO_2 (R) to VO_2 (M) is larger than on the switch from VO_2 (M) to VO_2 (R), given the kinetic asymmetry.

3.3. Comparing milled VO_2 particulate material to VO_2 particles from hydrothermal synthesis

In addition to bead milling of powders, a top-down method, also a bottom-up method such as hydrothermal synthesis can be applied to prepare sub-micron sized VO_2 (M) particles. To comparatively study the properties of milled and hydrothermally synthesized VO_2 particles, we prepared VO_2 particles by hydrothermal conversion of a vanadium(V) peroxo complex. This complex was prepared by reacting V_2O_5 and hydrogen peroxide in water. Subsequently, hydrazine was added as reducing agent, and the reaction mixture was converted to VO_2 nanoparticles in an autoclave at 220 °C for 72 h. After washing and drying of the solid product, its composition was analysed using XRD (Fig. S11). In addition to VO_2 (M) as the main crystalline product, the X-ray diffractogram displayed VO_2 (A) as a crystalline impurity. The SEM analyses predominantly showed spheroidal particles with an aspect ratio close to one, with a particle size of 62 ± 6 nm (Fig. 5d and e). In addition, a minor fraction of rods with a length and width of 1.60 ± 0.30 μm and 0.20 ± 0.04 μm were detected (Fig. 5d). Based on the typical rod-shaped structure of hydrothermally synthesized VO_2 (A) and the presence of VO_2 (A) as a crystalline impurity, the rods are most likely VO_2 (A) and the spheroidal particles VO_2 (M). To study the thermodynamic and kinetic characteristics of the SPT, we performed DSC analysis (Fig. 5a). These showed a ΔH of 31.8 J g^{-1}, which is slightly larger than ΔH of the smallest particles obtained by milling (29.1 J g^{-1}, particle size 129 ± 27 nm). T_0 for the SPT from VO_2 (M) to VO_2 (R) and *vice versa* were substantially lower for the hydrothermally synthesized particles, with 27.01 °C and 53.13 °C (Table 3) for the hydrothermally synthesized particles compared to 55.93 °C and 88.51 °C (Table 1) for the smallest bead milled ones. The hysteresis width, however, is large for both types of particles (26.12 °C for hydrothermally synthesized and 32.58 °C for smallest milled particles). DSC measurements and thermokinetic analysis were performed to determine the switching kinetics of the hydrothermally synthesized particles (Fig. 5b and c), using the same method as for milled particulate materials (*vide supra*). The results clearly demonstrate that $|E_\alpha|$ for the SPT of hydrothermally synthesized particles is in the same order of magnitude as for the smallest milled ones, albeit that the kinetic asymmetry is inversed. The switching kinetics of the hydrothermally synthesized particles are characterized by $|E_\alpha| = 267$ kJ mol^{-1} for the SPT from VO_2 (M) to VO_2 (R) and $|E_\alpha| = 755$ kJ mol^{-1} for the SPT from VO_2 (R) to VO_2 (M) at $\Delta T = 2.5$ °C. Whilst surface defects can be assumed to be induced by milling and play a key role in the switching kinetics of milled VO_2 particles, the switching characteristics of hydrothermally synthesized VO_2 may be dominated by bulk defects inside the VO_2 particles [46]. These different types of defects introduced using both preparatory techniques may explain the difference in kinetic asymmetry between both types of particles.

Table 2
Activation energy at $\Delta T = 2.5$ °C of the unmilled VO_2 powder sample and of the milled VO_2 particulate samples.

Milling energy [kWh·t^{-1}]	$\|E_\alpha\|$ [kJ·mol^{-1}]	
	VO_2 (M) to VO_2 (R)	VO_2 (R) to VO_2 (M)
0	1610	1491
3000	1225	1094
6000	748	897
9000	652	301
12000	517	237
13000	381	202

3.4. Thermochromic coatings consisting of milled VO_2 particulate material

To validate whether milled VO_2 particulate material has potential for application in thermochromic coatings, we deposited a layer of particulate material as thermochromic coating on glass. This layer was applied by dip coating a float glass sheet in a dispersion of milled VO_2 particulate material (particle size 129 ± 27 nm) in IPA, and subsequent drying of the coating under ambient conditions. Since the coating strongly absorbs blue light and contains particles with an average size above 100 nm that scatter light, the appearance of the coating is dark yellow and slightly opaque (Fig. 6a). SEM images of the coating show that it consists of a layer of VO_2 particles, and that stacking of these particles results in a porous coating (Fig. 6b and c). Furthermore, it can be observed that micron-sized spots of uncoated glass are still present after dip coating. To estimate the thickness of the coating, white light interferometry

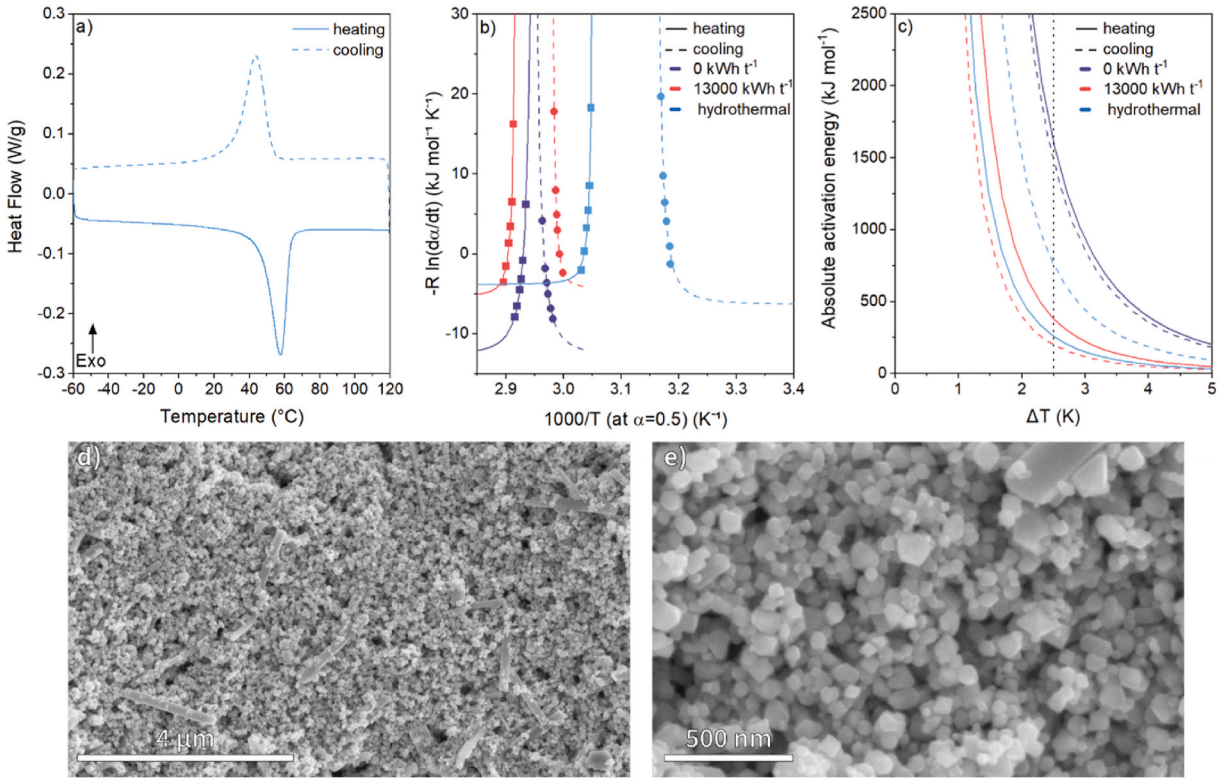

Fig. 5. a) DSC of hydrothermally synthesized VO_2 nanoparticles obtained at a heating/cooling rate of 5 °C·min^{-1}, b) Friedman plot for the hydrothermally synthesized VO_2 nanoparticles at $\alpha = 0.50$, c) comparing absolute activation energy of milled and hydrothermally synthesized VO_2 particles, d) and e) SEM images of hydrothermally synthesized VO_2 nanoparticles with different magnification of the sample.

Table 3
Temperature at 2 and 50% conversion of hydrothermally synthesized VO_2 nanoparticles measured at 5 °C·min^{-1} heating/cooling rate and average enthalpy for all heating/cooling rates (1.5, 5, 7.5 10, 15 and 20 °C·min^{-1}).

$T_{\alpha = 0.02}$ [°C]		$T_{\alpha = 0.50}$ [°C]		<ΔH> [J·g^{-1}]	
VO_2 (M) to VO_2 (R)	VO_2 (R) to VO_2 (M)	VO_2 (M) to VO_2 (R)	VO_2 (R) to VO_2 (M)	VO_2 (M) to VO_2 (R)	VO_2 (R) to VO_2 (M)
27.01	53.13	55.39	42.09	31.2 ± 0.04	32.4 ± 0.2

measurements were carried out (Fig. 6e and f). Optical profilometry (Fig. 6e) was used to measure the profile and average thickness of the VO_2 layer applied to a silicon wafer. Comparing the uncoated substrate and the coating leads to a resulting average thickness of 86 nm and a large surface roughness of 132 nm. *Ergo*, 86 nm is the average thickness of the coating derived from the very rough surface profile with large peak-valley distances.

UV–vis–NIR spectrophotometric analysis was carried out to optically characterize the coating, both at a temperature of 20 °C and 120 °C (Fig. 7a). The resulting spectra clearly show that the coating, solely consisting of milled VO_2 particulate materials, switches from a high transmission in the infrared (IR) part of the spectrum to a low solar IR transmission when increasing the temperature from below to above T_0. ΔT_{sol} for the coating is 8.3%. Specular reflection, diffuse reflection and diffuse transmission also change upon switching (Fig. S12). The difference in transmission for $\lambda = 1600$ nm is 30.2% (Fig. 7a), the transmission in the visible did not change ($T_{lum} = 40.7\%$ in both states, Fig. 7a). Based on these results, it is clear that the VO_2 particles display the SPT when applied to float glass as coating. Furthermore, using the temperature-controlled module in the UV–vis–NIR spectrophotometer with a heating rate of 1.75 °C·min^{-1} the switching kinetics of the VO_2 particle coating were analysed (Fig. 7b and c). For the conversion of VO_2 (M) to VO_2 (R), the rate of switching for the particulate material (heating rate 1.5 °C min^{-1}) and the coating are 0.14 min^{-1} and 0.10 min^{-1}, respectively. The difference in heating rate and the relatively large inaccuracy in heating of the coated glass plate in the UV–vis–NIR spectrophotometer may account for the rate difference. For the conversion of VO_2 (R) to VO_2 (M), the obtained rates for the milled particulate material and coating showed no significant difference (both 0.12 min^{-1}). Overall, these results clearly demonstrate that milled VO_2 particulate material has potential for application in thermochromic coatings. Optimization of the milling process, however, is required to further reduce the size and minimize the loss in crystallinity of the particulate material. This can be expected to lead to improved optical performance of the particle layers with an improved balance between T_{lum} and ΔT_{sol}. This performance increase is required to proceed towards thermochromic coatings with commercial potential [8].

4. Conclusion

We studied the key thermodynamic and kinetic characteristics of bead milled VO_2 particulate materials to validate whether they have potential for application in thermochromic coatings. We demonstrated that micron-sized VO_2 (M) powder could be successfully milled in IPA, and ultimately obtained nanoparticles of a size of 129 ± 27 nm. With progressive milling, not only the particle size, but also the switching enthalpy decreased. ΔH decreased from 46.8 J g^{-1} (unmilled powder) to 28.1 J g^{-1} (129 nm nanoparticles), which was caused by a loss in crystallinity of VO_2 of 20%–40% during milling. Milled nanoparticles display a higher switching rate than the unmilled powder. Progressive milling causes a gradual increase in switching rate of the nanoparticles, and induces kinetic asymmetry. For milled particles, the SPT from VO_2 (M) to VO_2 (R) proceeds significantly slower than the SPT from VO_2 (R) to VO_2 (M), whilst the unmilled powder showed almost no kinetic asymmetry. The activation energy for the SPT of hydrothermally

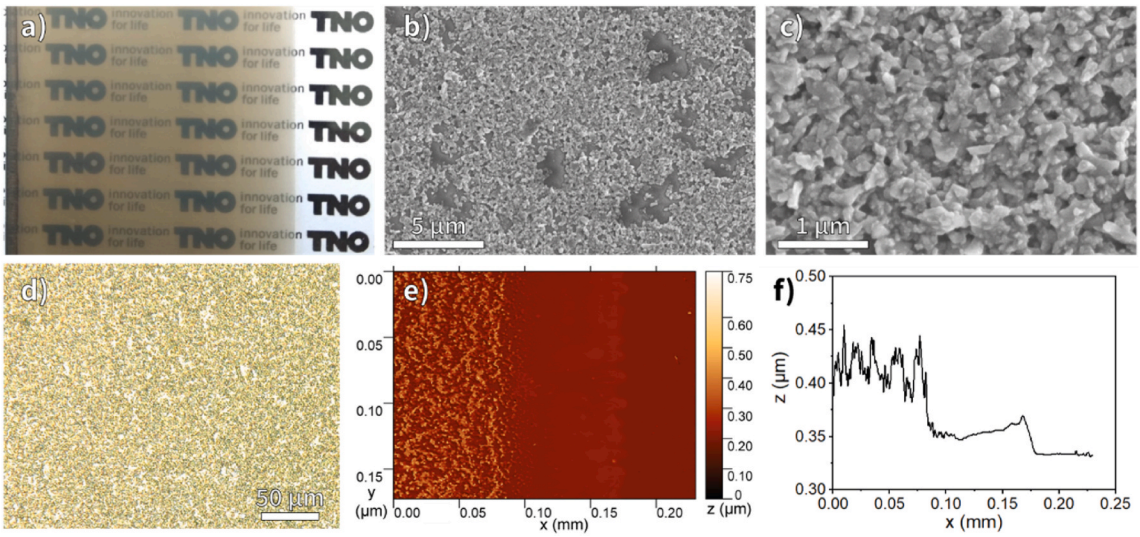

Fig. 6. a) Thermochromic coating on float glass, b) SEM image of coating on glass, c) SEM at higher magnification of the coating on glass, d) optical microscopy image of the coating on glass, e) optical profilometry of the coating on silicon wafer, and f) average surface roughness profile (z) extracted from the optical profilometry. (For interpretation of the references to colour in this figure legend, the reader is referred to the Web version of this article.)

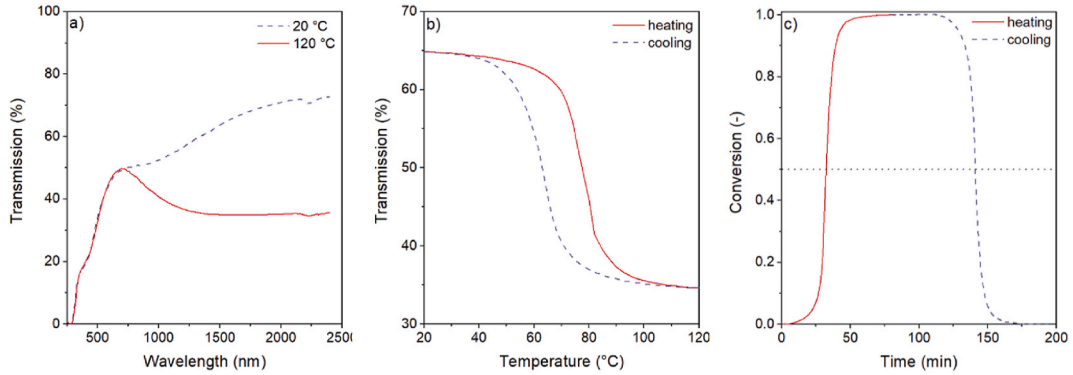

Fig. 7. a) UV–vis–NIR transmission spectra measured at 20 °C and 120 °C for the thermochromic particle-based coating, b) Transmission at $\lambda = 1600$ nm of the VO_2 coating as function of temperature upon heating and cooling with a rate of approximately 1.75 °C·min^{-1} and c) conversion-time profile for the VO_2 (M) to VO_2 (R) SPT of the coating and *vice versa* (obtained using changing transmission values at $\lambda = 1600$ nm).

synthesized VO_2 nanoparticles (62 ± 6 nm) was determined to be in the same range as for nanoparticles obtained by milling (129 nm). The kinetic asymmetry, however, was inverse to that of their bead milled counterparts. Whilst surface defects can be assumed to be induced by milling and play a key role in the switching kinetics of milled VO_2 particles, the switching characteristics of hydrothermally synthesized VO_2 may be dominated by bulk defects inside the VO_2 nanoparticles. These different types of defects introduced using both preparatory techniques may explain the difference in kinetic asymmetry between both types of particles.

Porous coatings prepared by stacking of milled VO_2 nanoparticles (129 nm) on float glass sheets by dip coating displayed thermochromic properties that are of interest for energy efficient windows. Coatings of an average thickness of 86 nm and a high surface roughness displayed a luminous transmission of 40.7% in both the cold and hot state. The transmission in the solar infrared, however, changed strongly resulting in a solar modulation of 8.3%. The switching rate of the coating was studied and yielded similar results as for the VO_2 particulate materials. Based on these results, it is clear that the VO_2 particles display the SPT when applied to float glass as a coating. Overall, the results presented in this manuscript demonstrate that milled VO_2 particulate material has potential for application in thermochromic coatings. Future work will focus on optimization of the milling process to further reduce the size and minimize the loss in crystallinity of the particulate material. This can be expected to lead to improved optical performance of the particle layers with an improved balance between T_{lum} and ΔT_{sol}, which is required to proceed towards thermochromic coatings with commercial potential. Furthermore, future work will focus on reducing the switching temperature of VO_2 (M) powders and particulate materials to 20–25 °C by doping with W^{6+}, which is required for application in thermochromic windows.

CRediT authorship contribution statement

Lavinia Calvi: Writing – original draft, Visualization, Validation, Methodology, Investigation, Formal analysis, Data curation, Conceptualization. **Romy van Geijn:** Investigation, Formal analysis, Data curation. **Luc Leufkens:** Formal analysis, Data curation. **Roberto Habets:** Writing – review & editing, Investigation, Formal analysis, Data curation. **Kargal Laxminarayana Gurunatha:** Writing – review & editing, Writing – original draft, Visualization, Validation, Methodology, Investigation, Formal analysis, Data curation, Conceptualization. **Kathleen Stout:** Writing – review & editing, Supervision, Conceptualization. **Daniel Mann:** Writing – review & editing, Methodology, Formal analysis, Data curation, Conceptualization. **Ioannis Papakonstantinou:** Writing – review & editing, Supervision, Resources, Funding acquisition,

Conceptualization. **Ivan P. Parkin:** Writing – review & editing, Funding acquisition, Conceptualization. **Ken Elen:** Writing – review & editing, Supervision, Formal analysis, Conceptualization. **An Hardy:** Writing – review & editing, Supervision, Resources, Investigation, Conceptualization. **Marlies K. van Bael:** Writing – review & editing, Supervision, Resources, Funding acquisition, Conceptualization. **Pascal Buskens:** Writing – review & editing, Writing – original draft, Supervision, Resources, Methodology, Funding acquisition, Conceptualization.

Declaration of competing interest

The authors declare that they have no known competing financial interests or personal relationships that could have appeared to influence the work reported in this paper.

Acknowledgements

The authors thank NWO-SIA (RAAK-PRO project Window of the Future) for their financial support. The authors acknowledge financial support from the European Fund for Regional Development through the cross-border collaborative Interreg V program Flanders-The Netherlands (project SUNOVATE), co-financed by the Belgian province of Limburg and the Dutch provinces of Limburg and Noord-Brabant. Furthermore, the authors gratefully acknowledge Dr. Marcel Verheijen (Eindhoven University of Technology and Eurofins Materials Science) for the TEM analyses, Dr. Martijn Brouwer and Dr. Man Xu (both TNO) for the optical profilometry measurements and Dr. Marta Jezierska-Switala (TNO) for the XRD analyses.

Appendix A. Supplementary data

Supplementary data to this article can be found online at https://doi.org/10.1016/j.solmat.2022.111783.

References

[1] M.E.A. Warwick, R. Binions, Advances in thermochromic vanadium dioxide films, J. Mater. Chem. A. 2 (2014) 3275–3292, https://doi.org/10.1039/c3ta14124a.
[2] S.-Y. Li, G.A. Niklasson, C.G. Granqvist, Thermochromic fenestration with VO2-based materials: three challenges and how they can be met, Thin Solid Films 520 (2012) 3823–3828, https://doi.org/10.1016/j.tsf.2011.10.053.
[3] A. Krammer, A. Matilainen, K. Pischow, A. Schüler, VO2:Ge based thermochromic solar absorber coatings, Sol. Energy Mater. Sol. Cells 240 (2022) 111680, https://doi.org/10.1016/j.solmat.2022.111680.
[4] Q. Xu, Y. Ke, C. Feng, C. Chen, Z. Wen, H. Wang, M. Sun, X. Liu, H. Liu, S. Magdassi, H. Li, C. Huang, Y. Long, Anisotropic localized surface plasmon resonance of vanadium dioxide rods in flexible thermochromic film towards multifunctionality, Sol. Energy Mater. Sol. Cells 230 (2021) 111163, https://doi.org/10.1016/j.solmat.2021.111163.
[5] J.L. Victor, C. Marcel, L. Sauques, N. Penin, A. Rougier, High quality thermochromic VO2 thin films deposited at room temperature by balanced and unbalanced HiPIMS, Sol. Energy Mater. Sol. Cells 227 (2021) 111113, https://doi.org/10.1016/j.solmat.2021.111113.
[6] C.N. Berglund, H.J. Guggenheim, Electronic properties of VO2 near the semiconductor-metal transition, Phys. Rev. 185 (1969) 1022–1033, https://doi.org/10.1103/PhysRev.185.1022.
[7] D. Mann, C. Yeung, R. Habets, Z. Vroon, P. Buskens, Comparative building energy simulation study of static and thermochromically adaptive energy-efficient glazing in various climate regions, Energies 13 (2020) 2842, https://doi.org/10.3390/en13112842.
[8] M. Arnesano, G. Pandarese, M. Martarelli, F. Naspi, K.L. Gurunatha, C. Sol, M. Portnoi, F.V. Ramirez, I.P. Parkin, I. Papakonstantinou, G.M. Revel, Optimization of the thermochromic glazing design for curtain wall buildings based on experimental measurements and dynamic simulation, Sol. Energy 216 (2021) 14–25, https://doi.org/10.1016/j.solener.2021.01.013.
[9] C. Zhou, D. Li, Y. Tan, Y. Ke, S. Wang, Y. Zhou, G. Liu, S. Wu, J. Peng, A. Li, S. Li, S. H. Chan, S. Magdassi, Y. Long, 3D printed smart windows for adaptive solar modulations, Adv. Opt. Mater. 8 (2020) 1–10, https://doi.org/10.1002/adom.202000013.
[10] B. Zhuang, Z. Dai, S. Pang, H. Xu, L. Sun, F. Ma, 3D ordered macroporous VO2 thin films with an efficient thermochromic modulation capability for advanced smart windows, Adv. Opt. Mater. 7 (2019) 1–9, https://doi.org/10.1002/adom.201900600.
[11] C.P.K. Yeung, R. Habets, L. Leufkens, F. Colberts, K. Stout, M. Verheijen, Z. Vroon, D. Mann, P. Buskens, Phase separation of VO2 and SiO2 on SiO2-Coated float glass yields robust thermochromic coating with unrivalled optical properties, Sol. Energy Mater. Sol. Cells 230 (2021) 111238, https://doi.org/10.1016/j.solmat.2021.111238.
[12] X. Lyu, A. Heßler, X. Wang, Y. Cao, L. Song, A. Ludwig, M. Wuttig, T. Taubner, Combining switchable phase-change materials and phase-transition materials for thermally regulated smart mid-infrared modulators, Adv. Opt. Mater. 9 (2021) 1–8, https://doi.org/10.1002/adom.202100417.
[13] F. Ding, S. Zhong, S.I. Bozhevolnyi, Vanadium dioxide integrated metasurfaces with switchable functionalities at terahertz frequencies, Adv. Opt. Mater. 6 (2018) 1–8, https://doi.org/10.1002/adom.201701204.
[14] C. Sol, M. Portnoi, T. Li, K.L. Gurunatha, J. Schläfer, S. Guldin, I.P. Parkin, I. Papakonstantinou, High-performance planar thin film thermochromic window via dynamic optical impedance matching, ACS Appl. Mater. Interfaces 12 (2020) 8140–8145, https://doi.org/10.1021/acsami.9b18920.
[15] C. Xu, G. Liu, M. Li, K. Li, Y. Luo, Y. Long, G. Li, Optical switching and nanothermochromic studies of VO2(M) nanoparticles prepared by mild thermolysis method, Mater, DES 187 (2020) 108396, https://doi.org/10.1016/j.matdes.2019.108396.
[16] I. Top, R. Binions, C. Sol, I. Papakonstantinou, M. Holdynski, S. Gaiaschi, I. Abrahams, Improved thermochromic properties in bilayer films of VO2 with ZnO, SnO2 and WO3 coatings for energy efficient glazing, J. Mater. Chem. C. 6 (2018) 12555–12565, https://doi.org/10.1039/c8tc04543g.
[17] V.P. Prasadam, N. Bahlawane, F. Mattelaer, G. Rampelberg, C. Detavernier, L. Fang, Y. Jiang, K. Martens, I.P. Parkin, I. Papakonstantinou, Atomic layer deposition of vanadium oxides: process and application review, Mater. Today Chem. 12 (2019) 396–423, https://doi.org/10.1016/j.mtchem.2019.03.004.
[18] S.Y. Li, G.A. Niklasson, C.G. Granqvist, Nanothermochromics: calculations for VO2 nanoparticles in dielectric hosts show much improved luminous transmittance and solar energy transmittance modulation, J. Appl. Phys. 108 (2010), 063525, https://doi.org/10.1063/1.3487980.
[19] S.Y. Li, G.A. Niklasson, C.G. Granqvist, Nanothermochromics with VO2-based core-shell structures: calculated luminous and solar optical properties, J. Appl. Phys. 109 (2011) 113515, https://doi.org/10.1063/1.3592350.
[20] C. Wang, H. Xu, C. Wang, T. Liu, S. Yang, Y. Nie, X. Guo, X. Ma, X. Jiang, Preparation of VO2 (M) nanoparticles with exemplary optical performance from VO2 (B) nanobelts by Ball Milling, J. Alloys Compd. 877 (2021) 159888, https://doi.org/10.1016/j.jallcom.2021.159888.
[21] F.Z. Shu, F.F. Yu, R.W. Peng, Y.Y. Zhu, B. Xiong, R.H. Fan, Z.H. Wang, Y. Liu, M. Wang, Dynamic plasmonic color generation based on phase transition of vanadium dioxide, Adv. Opt. Mater. 6 (2018) 1–10, https://doi.org/10.1002/adom.201700939.
[22] F. Wang, H. Chen, D. Lan, F. Zhang, Y. Sun, X. Zhang, S. Li, T. Cheng, Highly efficient and robust broadband nano-VO2(M) saturable absorber for nonlinear optics and ultrafast photonics, Adv. Opt. Mater. 9 (2021) 1–8, https://doi.org/10.1002/adom.202100795.
[23] J.L. Victor, M. Gaudon, N. Penin, A. Chiron, U.C. Chung, O. Viraphong, A. Rougier, Innovative sintering process for fabrication of thermochromic smooth VO2 ceramics, J. Alloys Compd. 890 (2021) 161890, https://doi.org/10.1016/j.jallcom.2021.161890.
[24] L. Calvi, L. Leufkens, C.P.K. Yeung, R. Habets, D. Mann, K. Elen, A. Hardy, M. K. Van Bael, P. Buskens, A comparative study on the switching kinetics of W/VO2 powders and VO2 coatings and their implications for thermochromic glazing, Sol. Energy Mater. Sol. Cells 224 (2021) 110977, https://doi.org/10.1016/j.solmat.2021.110977.
[25] Y. Cui, Y. Ke, C. Liu, Z. Chen, N. Wang, L. Zhang, Y. Zhou, S. Wang, Y. Gao, Y. Long, Thermochromic VO2 for energy-efficient smart windows, Joule 2 (2018) 1707–1746, https://doi.org/10.1016/j.joule.2018.06.018.
[26] K.L. Gurunatha, S. Sathasivam, J. Li, M. Portnoi, I.P. Parkin, I. Papakonstantinou, Combined effect of temperature induced strain and oxygen vacancy on metal-insulator transition of VO2 colloidal particles, Adv. Funct. Mater. 30 (2020) 1–9, https://doi.org/10.1002/adfm.202005311.
[27] M. Aburas, V. Soebarto, T. Williamson, R. Liang, H. Ebendorff-Heidepriem, Y. Wu, Thermochromic smart window technologies for building application: a review, Appl. Energy 255 (2019) 113522, https://doi.org/10.1016/j.apenergy.2019.113522.
[28] Z. Shao, X. Cao, H. Luo, P. Jin, Recent progress in the phase-transition mechanism and modulation of vanadium dioxide materials, NPG Asia Mater. 10 (2018) 581–605, https://doi.org/10.1038/s41427-018-0061-2.
[29] K. Liu, S. Lee, S. Yang, O. Delaire, J. Wu, Recent progresses on physics and applications of vanadium dioxide, Mater. Today 21 (2018) 875–896, https://doi.org/10.1016/j.mattod.2018.03.029.
[30] C. Liu, X. Cao, A. Kamyshny, J.Y. Law, S. Magdassi, Y. Long, VO2/Si-Al gel nanocomposite thermochromic smart foils: largely enhanced luminous transmittance and solar modulation, J. Colloid Interface Sci. 427 (2014) 49–53, https://doi.org/10.1016/j.jcis.2013.11.028.
[31] Y. Kim, S. Yu, J. Park, D. Yoon, A.M. Dayaghi, K.J. Kim, J.S. Ahn, J. Son, High-throughput roll-to-roll fabrication of flexible thermochromic coatings for smart windows with VO2 nanoparticles, J. Mater. Chem. C. 6 (2018) 3451–3458, https://doi.org/10.1039/c7tc05876d.
[32] X. Wang, M. Li, Q. Wang, J. Zhang, J. Shi, Y. Lu, G. Li, Effect of mie scattering on thermochromic performance of branched VO2 prepared by one-step hydrothermal method, Eur. J. Inorg. Chem. (2020) 1783–1789, https://doi.org/10.1002/ejic.202000123.
[33] Z. Chen, Y. Tang, A. Ji, L. Zhang, Y. Gao, Large-scale preparation of durable VO2 nanocomposite coatings, Appl. Nano Mater. 4 (2021) 4048–4054, https://doi.org/10.1021/acsanm.1c00387.

[34] S. Ji, F. Zhang, P. Jin, Preparation of high performance pure single phase VO2 nanopowder by hydrothermally reducing the V2O5 gel, Sol. Energy Mater. Sol. Cells 95 (2011) 3520–3526, https://doi.org/10.1016/j.solmat.2011.08.015.
[35] N. Wang, S. Magdassi, D. Mandler, Y. Long, Simple sol-gel process and one-step annealing of vanadium dioxide thin films: synthesis and thermochromic properties, Thin Solid Films 534 (2013) 594–598, https://doi.org/10.1016/j.tsf.2013.01.074.
[36] R. Chhabra, M.G. Basavaraj (Eds.), Coulson and Richardson's Chemical Engineering Volume 2A: Particulate Systems and Particle Technology, sixth ed., Butterworth-Heinemann, 2019.
[37] G.V. Chandrashekhar, H.L.C. Barros, J.M. Honig, Heat capacity of VO2 single crystals, Mater. Res. Bull. 8 (1973) 369–374, https://doi.org/10.1016/0025-5408(73)90039-1.
[38] P. Schilbe, D. Maurer, Lattice dynamics in VO2 near the metal-insulator transition, Mater. Sci. Eng. 370 (2004) 449–452, https://doi.org/10.1016/j.msea.2003.08.114.
[39] X. Xiao, H. Zhang, G. Chai, Y. Sun, T. Yang, H. Cheng, L. Chen, L. Miao, G. Xu, A cost-effective process to prepare VO2 (M) powder and films with superior thermochromic properties, Mater. Res. Bull. 51 (2014) 6–12, https://doi.org/10.1016/j.materresbull.2013.11.051.
[40] DIFFRAC.TOPAS | Bruker, (n.d.) (accessed April 22, 2022), https://www.bruker.com/en/products-and-solutions/diffractometers-and-scattering-systems/x-ray-diffractometers/diffrac-suite-software/diffrac-topas.html.
[41] S. Vyazovkin, N. Sbirrazzuoli, Isoconversional kinetic analysis of thermally stimulated processes in polymers, Macromol. Rapid Commun. 27 (2006) 1515–1532, https://doi.org/10.1002/marc.200600404.
[42] H.L. Friedman, New methods for evaluating kinetic parameters from thermal analysis data, Polym. Lett. 7 (1969) 41–46, https://doi.org/10.1002/pol.1969.110070109.
[43] S. Vyazovkin, Isoconversional Kinetics of Thermally Stimulated Processes, Springer, 2015.
[44] P. Papon, J. Leblond, P.H.E. Meijer, The Physics of Phase Transitions: Concepts and Applications, second ed., Springer, 2006 https://doi.org/10.1007/3-540-33390-8.
[45] H. Zhang, H. Yu, Z. Chen, H. Luo, Y. Gao, Thermal kinetic analysis of metal–insulator transition mechanism in W-doped VO2, J. Therm. Anal. Calorim. 126 (2016) 949–957, https://doi.org/10.1007/s10973-016-5579-3.
[46] J.-P. Duroudier, Grinding: principles and theories, in: Size Reduct. Divid. Solids, ISTE Press Ltd and Elsevier Ltd, 2016.